BIOCHEMISTRY
including biophysical chemistry & molecular biology
Article

Biochemistry **2009,** *48,* 6585–6597 6585
DOI: 10.1021/bi801827j

Guanidine Hydrochloride-Induced Unfolding of the Three Heme Coordination States of the CO-Sensing Transcription Factor, CooA[†]

Andrea J. Lee,[‡] Robert W. Clark,[‡] Hwan Youn,[§] Sarah Ponter,[‡] and Judith N. Burstyn*[,‡]

[‡]*Department of Chemistry, University of Wisconsin, Madison, Wisconsin 53706, and* [§]*Department of Bacteriology, University of Wisconsin, Madison, Wisconsin 53706*

Received September 26, 2008; Revised Manuscript Received October 24, 2008

ABSTRACT: CooA is a heme-dependent CO-sensing transcription factor that has three observable heme coordination states. There is some evidence that each CooA heme state has a distinct protein conformation; the goal of this study was to characterize these conformations by measuring their structural stabilities through guanidine hydrochloride (GuHCl) denaturation. By studying the denaturation processes of the Fe(III) state of WT CooA and several variants, we were able to characterize independent unfolding processes for each domain of CooA. This information was used to compare the unfolding profiles of various CooA heme activation states [Fe(III), Fe(II), and Fe(II)-CO] to show that the heme coordination state changes the stability of the effector binding domain. A mechanism consistent with the data predicts that all CooA coordination states and variants undergo unfolding of the DNA-binding domain between 2 and 3 M GuHCl with a free energy of unfolding of ~17 kJ/mol, while unfolding of the heme domain is variable and dependent on the heme coordination state. The findings support a model in which changes in heme ligation alter the structural stability of the heme domain and dimer interface but do not alter the stability of the DNA-binding domain. These studies provide evidence that the domains of transcription factors are modular and that allosteric signaling occurs through changes in the relative positions of the protein domains without affecting the structure of the DNA-binding region.

Allosteric activation of proteins is a process by which a change in protein activity is triggered by binding of an effector molecule. The induced-fit (or end-state) theory of allostery postulates that changes at the regulatory site of an allosteric protein induce a conformational change such that the inactive and active states of the protein are structurally distinct (*1*, *2*). Ideally, structural information collected in the presence and absence of effector molecule would allow for characterization of the structural requirements for protein activation. In reality, however, it can be difficult to acquire structures for all conformational states of a protein. Furthermore, a thorough understanding of protein allostery requires information about the thermodynamics of the transitions between these conformations, not just images of their static end points.

Heme dependent gas sensors are a burgeoning group of allosteric proteins with a wide range of sizes, domain architectures, and functions (*3*), yet it has been difficult to characterize the global structural changes that accompany effector binding among members of this group. In these proteins, the activation process is initiated by binding a gas molecule at the heme cofactor, and the structural and coordination rearrangements in the heme domain are transmitted to a domain that is responsible for activity of the protein. Studies of truncated heme domains have shed light on structural changes that occur in and around the heme pocket (*4*−*8*), but global conformational changes in heme-containing sensor proteins are largely uncharacterized due to the absence of crystal structures of full-length sensor proteins. Our best understanding of structure−function relationships in heme-containing gas sensors is based on studies of CooA,[1] the only gas sensor to be crystallized as a full-length polypeptide (*9*). Although several structures of CooA proteins exist (*10*, *11*), only one corresponds to the wild-type (WT) form of the protein in a physiologically relevant state (*9*). Many questions about allosteric regulation in CooA and heme-dependent sensors still remain to be answered. The most notable is how the signaling molecule cooperates with protein structural elements to transmit the allosteric signal and alter global protein structure.

[†]This work was supported by NIH Grant HL-66147 to J.N.B.

*To whom correspondence should be addressed. Telephone: (608) 262-0328. Fax: (608) 262-6143. E-mail: burstyn@chem.wisc.edu.

[1]Abbreviations: CooA, CO-sensing heme-containing transcription factor; GuHCl, guanidine hydrochloride; Fe(III) CooA, inactive form of *Rhodospirillum rubrum* CooA that has a ferric heme; Fe(II) CooA, inactive form of *R. rubrum* CooA that has a ferrous heme; Fe(II)-CO CooA, active form of *R. rubrum* CooA that has CO bound at the ferrous heme; WT, wild-type; F164W CooA, variant of WT CooA that has a substitution at position 164 (Phe → Trp); CODH, carbon monoxide dehydrogenase; CRP, cAMP receptor protein; FNR, fumarate nitrite reductase; MOPS, 3-(*N*-morpholino)propanesulfonic acid; PCR, polymerase chain reaction; DTT, dithiothreitol; CD, circular dichroism; PPIX, protoporphyrin IX; ΔG^{H_2O}, free energy of unfolding in the absence of denaturant; $\lambda_{max,F}$, wavelength of maximum intensity for a fluorescence spectrum; $\Delta\Delta G^{H_2O}$, difference in unfolding free energy measured for two proteins or two protein states.

Published on Web 06/24/2009

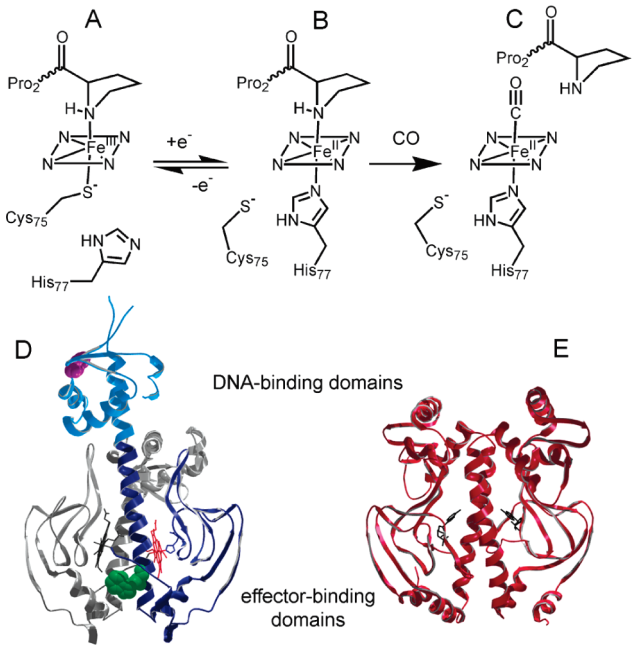

FIGURE 1: Heme activation states and structure of CooA. (A) In the Fe(III) state, the heme is ligated by Cys^{75} and Pro^{2} (proline is from the opposite monomer) (*15*−*17*). (B) When the heme is reduced, the Cys^{75} ligand is replaced with His^{77} (*9*, *15*, *18*, *19*). (C) CooA is activated when CO binds to the reduced heme, displacing the Pro^{2} ligand and enabling DNA binding (*20*). (D and E) Ribbon diagrams of the Fe(II) state of CooA (D) and CRP (E). Both proteins are dimers, with similar structure in the effector-binding and DNA-binding domains. CRP is in the active state with the cAMP effector bound and DNA-binding helices exposed for contact with DNA. CooA (one monomer in color) is in an inactive state, with the DNA-binding domains rotated such that the helices that contact DNA are solvent inaccessible. The effector domain of CooA is colored dark blue, while the DNA-binding domain is colored light blue. Trp^{110} (green) and Phe^{164} (purple) of CooA are shown with space-filled side chains; in F164W CooA, Phe^{164} is replaced with tryptophan. The truncated variant contains residues 1−132, which is the dark blue domain in this representation. This figure was prepared using PDB viewer and PDB entries 1FT9 and 1G6N (*9*, *24*).

Rhodospirillum rubrum (*Rr*) CooA is a CO-sensing transcription factor (*12*). In the presence of CO, CooA induces production of a carbon monoxide dehydrogenase (CODH) system that allows the organism to survive on CO as a sole energy source (*12*, *13*). CooA is a 49 kDa homodimer with an N-terminal effector-binding domain and a C-terminal DNA-binding domain that contains a helix−turn−helix motif (*9*). The effector domain of CooA contains two hemes (one in each monomer), and three heme activation states are known for *Rr* CooA (Figure 1). Under aerobic conditions, *Rr* CooA has a Fe(III) heme that is six-coordinate with a proximal cysteine ligand and a distal N-terminal proline ligand (*15*−*17*). This state is incapable of binding CO and is inactive for DNA binding. Upon reduction, CooA undergoes a proximal ligand switch from cysteine to histidine but retains the distal proline ligand (*9*, *15*, *18*, *19*). This state is poised for activation. Exposure of the reduced state to CO results in replacement of the distal proline to give a heme with histidine/CO coordination (*20*). The CO-bound state is active for binding to DNA (*12*, *21*, *22*). It has been suggested that CooA has three distinct conformations corresponding to the three heme coordination states (Figure 1) (*18*).

CooA is a member of the cAMP receptor protein (CRP)/fumarate nitrite reductase (FNR) family of homodimeric transcriptional regulators (*14*). Members of this family appear to have a common set of structural elements that are critical for allosteric activation. One of these elements is a coiled-coil dimer interface that has some degree of leucine zipper character (*9*, *23*, *24*). Evidence suggests that effector binding has a direct influence on residues at this dimer interface. Mutations in CooA that strengthen the leucine zipper interactions result in effector-independent DNA binding activity (*25*), and cAMP appears to regulate CRP through specific contacts with the residues at the dimer interface (*26*). The significance of the subunit interface is most obvious in FNR, which is regulated through a monomer−dimer equilibrium (*27*). Another common element is a "hinge" sequence that exists between the dimer interface and the DNA-binding domain. Mutagenesis of hinge residues has shown that flexibility in this region is essential for proper communication of the signal in both CooA and CRP (*9*, *28*−*32*).

It has been suggested that activation in CooA and CRP is dependent on repositioning of the DNA-binding domain through the hinge to allow exposure of a critical helix (the F helix) for contact with DNA. All studies of the inactive structures of CooA (*9*) and CRP (*33*, *34*) show the F helix is buried and unable to make contacts with DNA. Conversely, in the studies of the active states of CooA and CRP, the F helix is on the surface of the protein and exposed for interactions with DNA (*24*, *33*, *35*). The structure of active CRP in the presence of DNA clearly shows hydrogen bonding between three residues in each F helix and DNA (*36*, *37*), and mutations in the *Rr* CooA F helix at suspected H-bonding positions disrupted CooA−DNA interactions (*38*). In addition, many other studies of CooA and CRP activation have implicated an effector-dependent change in the position of the DNA-binding domain (*10*, *11*, *35*) (reviewed in ref *35*).

In this study, we sought to further characterize conformational differences among the activation states of a single member of the CRP family, *Rr* CooA. If global conformational changes occur in CooA, they might be expected to impart changes to the overall structural stability of the protein. A method that allows for measurement and comparison of protein stabilities is chemical denaturation (*39*), where differences in the slope, transition midpoints, and overall shape of the unfolding curves signify structural differences among proteins. Ligand binding has been shown to alter protein stability (*40*−*45*). Furthermore, heme proteins such as hemoglobin (*46*, *47*) and cytochrome *c* (*48*) have been unfolded in multiple heme coordination states, and stability differences have been observed. The studies reported herein were designed to measure possible variations in stability for the conformations that correspond to the three heme coordination states of *Rr* CooA.

We report here GuHCl unfolding studies of Fe(III) CooA monitored by visible, fluorescence, and CD spectroscopy. We used two CooA variants to explore the mechanism of unfolding in the WT protein: a truncated form of CooA that lacks the DNA-binding domain provided information specific to the heme domain, and F164W CooA, a variant containing an additional tryptophan fluorescence signal, provided information specific to the DNA-binding domain. We found that the domains of Fe(III) WT CooA and variants unfold independently, with distinct transitions that are easily visible in the unfolding curves. On the basis of the results from the variants, we were able to interpret the differences in the Fe(III), Fe(II), and Fe(II)-CO WT CooA denaturation curves. We fit these unfolding curves for multiple unfolding intermediates to generate free energy values that describe the stabilities of the CooA domains. Models describing

the denaturation process are presented which have implications for the function of both gas-sensing heme proteins and allosterically regulated transcription factors. Our findings demonstrate that domain modularity plays a role in signal transduction and activation in these proteins.

MATERIALS AND METHODS

Materials. MOPS was purchased from Sigma. Guanidine hydrochloride (ultrapure) was from ICN. Sodium dithionite was purchased from Fluka. Unless otherwise specified, all manipulations were carried out in 25 mM MOPS buffer (pH 7.4) with 100 mM NaCl.

Strains and Plasmids. The construction of strains overexpressing WT CooA in *Escherichia coli* backgrounds has been previously described (*18*, *25*). F164W CooA was overexpressed in strain UQ2412, which is a derivative of strain UQ1639 (*18*). F164W CooA was constructed in a pEXT20-based expression plasmid as previously described (*49*). Site-directed mutagenesis involved PCR amplification of CooA with primers designed to incorporate the desired nucleotide changes as described elsewhere (*50*).

Purification of WT, F164W, and Truncated CooA. WT CooA was purified to >95% as described previously (*18*) and stored at −80 °C in 25 mM MOPS buffer (pH 7.4) with 100 mM NaCl until use. F164W CooA was purified and stored using the same procedures. The CooA truncate was purified as described previously (*51*) and stored at −80 °C in 25 mM MOPS buffer (pH 7.4) with 750 mM NaCl, 10% glycerol, and 2 mM DTT. WT and F164W CooA had the same visible absorption spectrum and were assumed to have the same ε_{424} for the Fe(III) state. The protein concentration was determined by the extinction coefficient of the heme cofactor (ε_{424} = 105 mM^{-1} cm^{-1}) (*52*) or by bicinchoninic acid assays (*53*).

In Vitro Protein Activity Assays. Activity of WT and F164W CooA was measured at room temperature using a fluorescence polarization method (*49*). Briefly, a 26 bp target DNA containing pCooF was labeled with Texas Red on the 5′ end of one strand of the DNA. The labeled oligonucleotide was titrated with protein, and the protein−DNA complex was detected by an increase in fluorescence anisotropy. Dissociation constants were calculated by nonlinear least-squares fit (*54*).

Visible Absorption Spectroscopy. CooA unfolding was measured by the loss of intensity at the strongest band in the absorption spectrum (the Soret peak) with an increasing concentration of GuHCl. The Soret wavelengths used were 424 nm for Fe(III) WT, Fe(III) F164W, and Fe(III) truncate CooA; 425 nm for Fe(II) WT CooA; and 423 nm for Fe(II)-CO WT CooA (*51*, *52*). Visible absorption spectra were recorded at room temperature on a Varian Cary 4 Bio spectrophotometer with a bandwidth of 0.5 nm. Samples of protein (2 μM) or hemin (4 μM) were monitored over the full wavelength range (350−800 nm) to investigate heme changes. Intensity was measured using a cuvette with a path length of 1 cm.

CD Spectroscopy. CD experiments were performed at room temperature with an Aviv model 202SF stopped-flow CD spectrometer or an MOS-450 spectropolarimeter from BioLogic (BioLogic Science Instruments, Claix, France). CD spectra were measured over a range of 200−400 nm with a path length of 0.1 or 0.2 cm. Spectra were recorded in 1 nm increments with an averaging time of at least 1 s. Single-wavelength measurements were taken with an averaging time of 10 s. The protein concentration was 2 μM for all samples. CD data for WT CooA and F164W CooA were recorded in 25 mM MOPS, 100 mM NaCl, pH 7.4 buffer. The Fe(II) state for WT CooA was generated by the addition of a minimal amount of buffer containing dithionite to Ar-purged samples of the Fe(III) protein. The Fe(II)-CO state for WT CooA was prepared by addition of CO gas to the headspace of the corresponding Fe(II) sample. Conversion to the appropriate state (as well as minimal residual concentration of dithionite) was confirmed by visible absorption spectroscopy.

Fluorescence Spectroscopy. All fluorescence measurements were taken on an ISS PC1 photon counting fluorometer (ISS Instruments Inc., Champaign, IL) at room temperature. Data were recorded in a cuvette with a 2 mm excitation and a 1 cm emission path length. All protein samples were at a concentration of 2 μM. Emission spectra were recorded from 290 to 400 nm with excitation and emission slits of 1.0 mm. Corrections were made by subtracting the spectrum of the appropriate buffer. For titrations, an excitation wavelength of 296 nm was used to select for tryptophan fluorescence with excitation slits of 0.5 mm and emission slits of 2.0 mm. Samples were monitored at an emission wavelength of 352 nm (the wavelength of maximum intensity changes between 0 and 6.25 M GuHCl) to measure unfolding.

Titrations with Guanidine Hydrochloride. GuHCl stocks were prepared by dissolving solid denaturant in the buffer appropriate for storage of each protein, followed by filtration. Concentrations of denaturant were determined by refractive index (*55*). In each GuHCl denaturation experiment, 26 samples of CooA were titrated with GuHCl from 0 to 6.25 M, at a protein concentration of 2 μM, unless otherwise specified. Unfolding was intiated by dilution of a concentrated protein stock into the appropriate GuHCl buffer. All samples were incubated at room temperature for 2 h before measurement using the procedures outlined above. The data shown in Figures 2−4 are one representative data set, while Figure 5 shows raw intensity data with error bars representing the standard deviation from three measurements.

Fe(III) WT CooA titrations were carried out at different concentrations of protein. The samples were prepared using the titration conditions given above, but at 4, 2, or 0.5 μM protein. Changes in CooA were measured using visible absorbance, CD, and fluorescence as described.

Preparation and handling of the Fe(II) CooA and Fe(II)-CO CooA samples and titrations required special techniques for maintenance of the proper oxidation state. All buffers and GuHCl stock solutions were degassed by a first step of filtration through a 0.2 μm filter or centrifugation at 10000*g*, followed by a second step of purging with Ar gas. For Fe(II) CooA and Fe(II)-CO CooA titrations, the protein stock was reduced with solid $Na_2(S_2O_4)$ (dithionite) before it was titrated. For Fe(II)-CO CooA titrations, the Fe(II) CooA stock solution was exposed to CO gas in the headspace to form the CO adduct. Samples for unfolding titrations were prepared in a nitrogen-filled glovebox, using the methods described above. After incubation for 2 h in the glovebox, visible absorbance or CD spectra were measured for each sample. The presence of the appropriate heme coordination state was confirmed by visible absorption spectroscopy both immediately before addition of GuHCl to the samples and immediately before measurement of unfolding by the requisite spectroscopic method.

Measurement of fluorescence unfolding curves for Fe(II)-CO WT and Fe(II)-CO F164W CooA required removal of excess

dithionite reductant. Dithionite quenches tryptophan fluorescence; however, quenching does not occur when the reductant is fully oxidized. Fluorescence spectroscopy is possible for the Fe(II)-CO state of CooA due to the slow CO off rates for Fe(II)-CO CooA, and CO-bound samples may be exposed to an aerobic environment without a change in heme coordination. To measure the fluorescence of the CO adduct, we exposed the samples to air to allow for oxidation of the dithionite immediately before measurement of tryptophan fluorescence. The presence of the appropriate heme coordination state and complete removal of dithionite were confirmed by visible absorption spectroscopy immediately prior to measurement of fluorescence. The same techniques cannot be used for detection of fluorescence in Fe(II) WT CooA because the protein reoxidizes readily in the absence of reductant.

Reversibility. Fe(III) WT CooA cannot be diluted from 6 to 0 M GuHCl without precipitation. In an exemplary experiment, a sample of 50 μM Fe(III) WT CooA and 6 M GuHCl was allowed to unfold for 2 h at room temperature before being placed in a Float-A-Lyzer (Spectrum Laboratories) regenerated cellulose dialysis cartridge with a molecular mass cutoff of 10000 Da. The sample was then dialyzed against two changes of 2 M GuHCl before being dialyzed against 0 M GuHCl buffer. Precipitation was observed when the protein was dialyzed against GuHCl concentrations of <0.5 M, and visible absorption spectra indicated that the heme environment of the refolded Fe(III) WT CooA was severely perturbed.

A titration−dilution method was pursued to investigate reversibility in the CD and fluorescence spectra. WT Fe(III) CooA (50 μM) was denatured for 2 h at a GuHCl concentration of 5 M at room temperature. The presence of unfolded CooA was confirmed through visible spectroscopy. The protein was then diluted to 2 μM and the final GuHCl concentration desired and allowed to incubate for 2 h at room temperature. An elevated fluorescence signal was observed for dilution from 5 to <3 M GuHCl; therefore, a separate dilution was carried out from 3 to 0.5 M GuHCl. Only in CD spectroscopy did we observe full recovery of the signal, indicating the refolding of the secondary structure between 5 and 0.5 M GuHCl. Persistent precipitation below 0.5 M GuHCl prevented investigation of the activity of the renatured protein, as high concentrations of salt interfere with the CooA activity assay.

Quaternary Structure Measurements. GuHCl-induced unfolding of WT Fe(III) CooA was analyzed by size exclusion chromatography using a Superdex 75 prepacked column (16 mm$\times$600 mm; gel volume of 120 mL; GE). The high GuHCl concentrations greatly perturbed the elution times for CooA, and calibration using molecular weight standards confirmed that protein separation was not adequate for analysis of CooA quaternary structure at 5 M GuHCl. Furthermore, size exclusion chromatography was not possible for Fe(II) or Fe(II)-CO CooA, each of which requires reducing conditions to maintain the heme states. Other methods, such as analytical ultracentrifugation, were unsuccessful for analysis of the CooA quaternary state due to the formation of aggregates.

Analysis of Denaturation Data. The analysis of two-state unfolding behavior using linear extrapolation has been described previously (*56*), and we used the standard two-state methods and equations to analyze visible absorbance data for all protein variants and states and CD unfolding data for Fe(III) truncated CooA. Briefly, the pre- and post-transition baseline slopes and intercepts were fitted using a linear least-squares regression, and these parameters were fixed while the free energy (ΔG^{H_2O}) and slope (m) for each curve were fitted to the equations described using linear extrapolation (*57*).

CD data for Fe(III) WT, Fe(III) F164W, Fe(II) WT, and Fe(II)-CO CooA were fitted to a three-state model with a single intermediate, and all fluorescence data were fitted to a four-state model with two intermediates (see below). The choice of a model was based on (i) evidence for multiple states in the full-wavelength visible absorption spectra, (ii) the presence of an intermediate indicated by irreversibility of unfolding, and (iii) use of the fewest states that could reasonably fit the obvious transitions in the unfolding curves. Several models are possible for the unfolding process of CooA, but we chose the simplest model that would allow for comparison of unfolding curves and determination of relative values for the free energy of unfolding among CooA states and variants.

Although the four-state model is presented below, the three-state fits follow the same method but include only one intermediate. The four-state model assumed for the unfolding of Fe(III) WT CooA is shown in eq 1.

$$F \rightleftharpoons I \rightleftharpoons J \rightleftharpoons D \tag{1}$$

Using this model, equilibrium constants are defined for the folding processes, in which denatured state D folds to each successive species, as shown in eqs 2−4.

$$K_{DF} = [F]/[D] \tag{2}$$

$$K_{DI} = [I]/[D] \tag{3}$$

$$K_{DJ} = [J]/[D] \tag{4}$$

The observed signal is proportional to the signal intensity of the species (Y), corrected for the fractional population of each state (f) (eq 5)

$$Y_{obs} = f_F Y_F + f_I Y_I + f_J Y_J + f_D Y_D \tag{5}$$

and the fraction of each state is related to the concentration of the state over the sum of all species (eqs 6−9).

$$f_F = [F]/([F]+[I]+[J]+[D]) \tag{6}$$

$$f_I = [I]/([F]+[I]+[J]+[D]) \tag{7}$$

$$f_J = [J]/([F]+[I]+[J]+[D]) \tag{8}$$

$$f_D = [D]/([F]+[I]+[J]+[D]) \tag{9}$$

If the fraction of folded protein is taken as an example, these fractions are related to the equilibrium constants by eq 10.

$$\begin{aligned} f_F &= ([F]/[D])/([F]/[D]+[I]/[D]+[J]/[D]+[D]/[D]) \\ &= K_{DF}/(K_{DF}+K_{DI}+K_{DJ}+1) \end{aligned} \tag{10}$$

The equilibrium constant at each guanidinium hydrochloride concentration for each folding process (D $\rightarrow$ F, D $\rightarrow$ I, and D $\rightarrow$ J) is related to the free energy of this process. Using the linear regression method for analysis of denaturation data (*56*), eq 5 may be rearranged to give an expression for total spectral intensity in terms of ΔG^{H_2O} and slope of each folding process.

The data for total intensity were fitted by fixing the intensity of each intermediate and varying the ΔG^{H_2O} and slope for each folding process. The error between the calculated intensity and the measured data was minimized using nonlinear least-squares regression. The values reported for the free energy change between the folded protein and the intermediates (ΔG_{FI}, ΔG_{IJ}, and ΔG_{JD}) were acquired by calculating the difference between the free energy of each folding process and the free energy of the conversion from the folded to denatured protein (e.g., $\Delta G_{FI} = \Delta G_{DI} - \Delta G_{DF}$). Typically, the free energy values collected from these fits were correlated, but starting free energy values and spectral intensities for intermediates that were derived from the two-state fits for domain stability and the observed spectra of the above protein variants were used. The data were fitted to give the free energy of folding in the absence of denaturant but are presented as the free energy of unfolding (ΔG^{H_2O}) in Table 1 for the sake of clarity.

RESULTS

Visible Absorption Spectroscopy Allows for Observation of Unfolding of the Effector Domain in Fe(III) WT and Fe(III) Variant CooA Proteins. The heme of CooA presents an opportunity to follow protein unfolding using visible absorption spectroscopy to monitor changes in protein environment around the cofactor. Visible absorbance data for the unfolding of Fe(III) WT CooA show the presence of at least one intermediate heme state during the unfolding process (Figure 2A). Fe(III) WT CooA has a Soret peak in the visible spectrum at 424 nm that disappears with increasing concentrations of GuHCl. From 0 to 3.75 M GuHCl, the heme spectra exhibit an isosbestic change in absorbance marked by the disappearance of the strong Soret band at 424 nm and the growth of a broad band at roughly 360 nm. These spectra then show a second isosbestic change between 3.75 and 6.25 M GuHCl. The final spectrum of unfolded Fe(III) WT CooA is similar to that of Fe(III) PPIX in 6.25 M GuHCl (data not shown). The absorbance unfolding profile of Fe(III) WT CooA shows an unfolding transition between 3 and 4 M GuHCl (Figure 2B). Visible absorbance unfolding curves for titrations of Fe(III) WT CooA at 2 and 4 μM were the same; however, at protein concentrations of 0.5 μM, the unfolding curves exhibit transition regions that occur at lower concentrations of GuHCl than those at 2 and 4 μM. At 4 μM protein, the unfolding curve shows a decrease in intensity in the pretransition region (Figure 2B). We attribute these pretransition changes to alterations in the heme environment at low concentrations of GuHCl (<3 M) due to unfolding of the DNA binding region (vide infra).

We unfolded two protein variants to aid in characterization of the CooA unfolding process. The first variant that was unfolded is a truncated version of Fe(III) CooA that contains residues 1−132 of the WT protein. The truncated protein consists of only the heme domain of CooA and has been crystallized as a dimer with a structure almost identical to that of the heme domain of the WT protein (*51*). The Fe(III) truncated version of CooA shows a visible absorbance unfolding transition that occurs in the same GuHCl concentration range as that of Fe(III) WT CooA, signifying that removal of the DNA-binding domain has virtually no effect on the stability of the heme domain as observed through visible spectroscopy. Unlike Fe(III) WT CooA, the Fe(III) truncate shows minimal intensity changes between 0 and 3 M GuHCl, indicating that that the decrease exhibited by WT Fe(III) CooA at these concentrations may be related to an unfolding process in the DNA-binding domain.

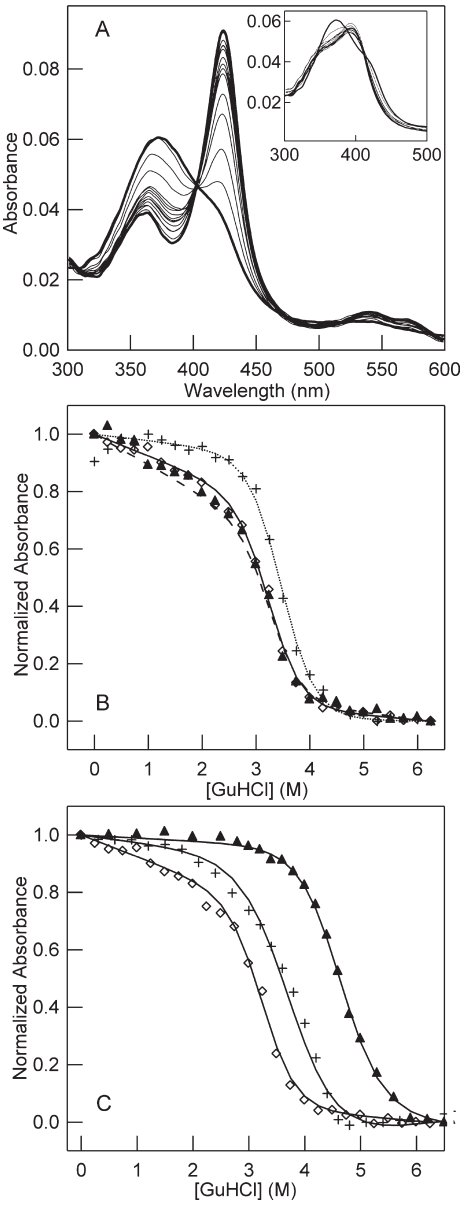

FIGURE 2: Denaturation of CooA monitored by visible spectroscopy of the heme for WT and variants of CooA in the Fe(III) state (A and B) and the Fe(II) and Fe(II)-CO states of WT CooA (C). Samples with a fixed protein concentration (2 μM) were titrated with GuHCl from 0 to 6.25 M and allowed to unfold for 2 h at 25 °C before the full absorption spectrum was recorded. Lines represent fits to a two-state unfolding model for all proteins and variants. (A) Visible absorption spectra of Fe(III) WT CooA exhibit isosbestic changes between 0 and 3.75 M GuHCl. Samples between 3.75 and 6 M GuHCl show an additional isosbestic transition (inset of panel A). (B) Changes in Soret intensity at 424 nm as a function of an increasing GuHCl concentration for Fe(III) WT (◇), Fe(III) F164W (▲), and Fe(III) truncated CooA (+). (C) Changes in the absorbance intensity of Fe (III) WT (◇), Fe(II) WT (+), and Fe(II)-CO WT (▲) CooA at the Soret peak for each species (424, 425, and 423 nm, respectively) as a function of GuHCl concentration.

The second variant, Fe(III) F164W CooA, has a substitution to provide an additional tryptophan fluorescence signal in the DNA-binding domain and was selected to help in interpretation of the fluorescence unfolding data (see below). The mutated residue is far from the heme domain (Figure 1D) and has no effect on the native absorbance, fluorescence, or CD spectrum of the

protein (see Figure S1 of the Supporting Information for CD spectra). As expected, the Fe(III) F164W variant shows the same visible absorbance unfolding profile as the Fe(III) WT protein (Figure 2B). Taken together, these results suggest that (i) the heme domain of Fe(III) CooA is a structural unit that unfolds between 3 and 4 M GuHCl regardless of the absence or presence of a DNA-binding domain, (ii) visible absorbance data primarily reflect changes in the heme domain, and (iii) the slope in the pretransition region of the Fe(III) WT CooA curve appears to be correlated with changes in the DNA-binding domain.

Changes in the Heme Ligation and Activation State of CooA Affect the Unfolding of the Heme Domain. To detect possible differences in the structural stability of the various heme coordination states of CooA, we compared visible absorbance changes that accompany GuHCl denaturation of Fe(II)-CO, Fe(II), and Fe(III) WT CooA (Figure 2C). Upon titration of Fe(II)-CO WT CooA with an increasing concentration of GuHCl, the Soret peak at 423 nm in the visible absorption spectrum converts isosbestically to a peak at 410 nm, and the final state (6.25 M GuHCl) has a spectrum that appears to be the same as that of Fe(II)-CO protoporphyrin IX (PPIX) in 6.25 M GuHCl solution (data not shown). The visible absorbance unfolding profile of Fe(II)-CO WT CooA differs from that of Fe(III) WT CooA in that the Fe(II)-CO Soret peak shows a large decrease in absorbance intensity between 4 and 5 M GuHCl (Figure 2C).

The Fe(II) WT CooA visible unfolding profile differs from both the Fe(II)-CO WT and Fe(III) WT unfolding curves. Exposure of Fe(II) WT CooA to increasing concentrations of GuHCl causes a decrease in the intensity of the Soret peak at 425 nm, and the final state appears to be the same as free Fe(II) PPIX in 6.25 M GuHCl (data not shown). The Soret absorbance intensity of Fe(II) WT CooA starts to show significant decreases at 2 M GuHCl that continue until 4.75 M GuHCl (Figure 2C). These data would suggest that the Fe(II) WT CooA heme domain has stability to GuHCl denaturation that is intermediate between the lower stability of Fe(III) WT CooA and the higher stability of Fe(II)-CO WT CooA.

The increased stability of the Fe(II)-CO heme domain as compared to the Fe(III) state is not derived from changes in the DNA-binding domain. We titrated the Fe(II)-CO state of truncated CooA (residues 1−132) with GuHCl (data not shown), and the absorbance intensity of the CO-bound form of the variant showed no change between 0 and 4.5 M denaturant. Fe (II)-CO truncate CooA exhibited a folding transition between 4.5 and 6 M denaturant, which is within a concentration range much higher than the transition observed for the Fe(III) truncate CooA (3−4 M). This result suggests that the visible absorbance unfolding curves for the WT CooA protein correlate to the relative stability of the heme domain in the three states of CooA and are unrelated to the presence of the DNA-binding domain.

The visible absorbance data for unfolding of the various states and variants of CooA were fitted to a two-state model according to published methods (Table 1) (*56*). These fits give a relatively consistent ΔG^{H_2O} (free energy of unfolding in the absence of denaturant) of ~27 kJ/mol for Fe(III) WT, Fe(III) truncated, and Fe(III) F164W CooA. Fits for the Fe(II)-CO WT CooA and Fe(II) WT CooA absorbance unfolding curves give ΔG^{H_2O} values of 29 and 22 kJ/mol, respectively.

CD Spectroscopy Allows for Observation of Unfolding of the Heme- and DNA-Binding Domains of Fe(III) WT CooA. Monitoring the CD spectrum of CooA as a function of GuHCl concentration is a logical way to examine unfolding of both domains of the WT protein. The DNA-binding domain of CooA is rich in α-helix, and the protein dimer interface in the effector-binding domain is a long α-helical leucine-zipper motif. Both of these domains are expected to contribute to the native CD signal at 222 nm. A comparison of the native CD spectrum of Fe(III) WT and Fe(III) truncate CooA (Figure S1 of the Supporting Information) shows the variant to have a much weaker intensity at 222 nm, presumably because the variant lacks the signal component that is derived from the helix−turn−helix motif.

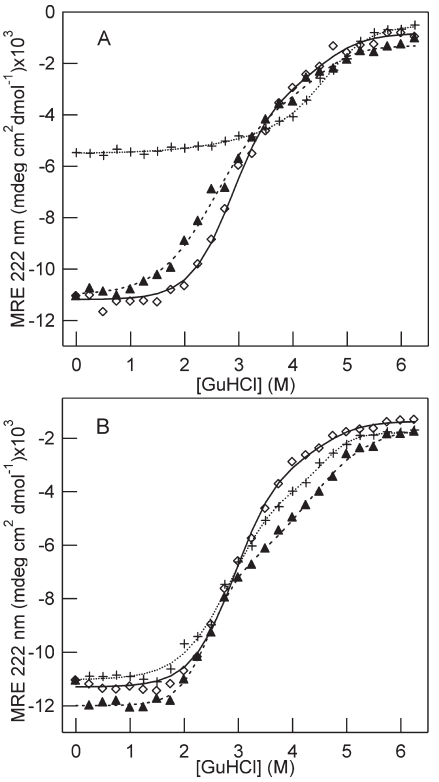

FIGURE 3: Denaturation of CooA monitored by CD spectroscopy for Fe(III) WT, Fe(III) F164W, and Fe(III) truncated CooA (A) and Fe(II) WT and Fe(II)-CO WT CooA (B). Samples of a fixed concentration of CooA (2 μM) were titrated with GuHCl from 0 to 6.25 M and were allowed to unfold for 2 h at 25 °C before the measurement of CD intensity. The CD intensity at 222 nm is plotted as a function of GuHCl concentration. The solid curves represent fits to a three-state model in the case of WT and F164W CooA and a two-state model in the case of Fe(III) truncated CooA. (A) Unfolding curves for Fe(III) WT (◇), Fe(III) F164W (▲), and Fe(III) CooA truncation variant (+) consisting only of the heme domain. (B) Unfolding curves for Fe(III) (◇), Fe(II) (+), and Fe(II)-CO (▲) WT CooA.

The CD spectrum of Fe(III) WT CooA shows a decrease in intensity with an increase in GuHCl concentration, consistent with unfolding of α-helix in the protein. The greatest change in CD signal occurs in a range of GuHCl concentrations [2−4 M GuHCl (Figure 3A)] that differs from that observed for the Fe(III) WT visible absorbance unfolding curves [>3 M (Figure 2B)]. The CD intensity shows changes over a broad range of GuHCl concentrations, possibly because CD data reflect the unfolding of both CooA domains. The CD unfolding profile exhibited little concentration dependence for all studied protein concentrations. CD profiles for unfolding of Fe(III) F164W CooA are comparable to the profiles for Fe(III) WT CooA (Figure 3A), which suggests similar unfolding processes.

To account for the contribution of each domain to the unfolding of Fe(III) WT CooA, we unfolded the Fe(III) truncated variant of CooA, which lacks the helix−turn−helix DNA-binding domain. The CD unfolding curve of the truncated variant is substantially different from that of the full-length Fe(III) WT CooA protein (Figure 3A); changes for Fe(III) truncate CooA do not occur until 4 M GuHCl, and the profile shows a single unfolding transition. No changes are observed between 2 and 3 M GuHCl in the truncate CooA CD unfolding profile, indicating that the effector domain is stable in this GuHCl concentration range. These results support the proposal that the Fe(III) WT CooA DNA-binding domain unfolds between 2 and 3 M GuHCl.

Heme-Dependent Changes in CooA Structure Result in Differences in CD Unfolding Curves at High Concentrations of GuHCl. To detect possible differences in the stability of the α-helix in the various heme coordination states of CooA, we carried out GuHCl denaturation studies with Fe(II) and Fe(II)-CO WT CooA and monitored the CD signal at 222 nm. CD spectra of three heme coordination states of CooA show minimal differences in α-helical secondary structure (Figure S1 of the Supporting Information). Upon titration with GuHCl, the CD spectra of Fe(II) and Fe(II)-CO WT CooA both show a decrease in intensity, indicating a loss of α-helical secondary structure. A comparison of the CD unfolding profiles at 222 nm of the three heme states of WT CooA (Figure 3B) indicates that the states show similar changes in CD intensity at GuHCl concentrations of < 3 M, and all states show an unfolding transition in the CD data that covers a broad range of GuHCl concentrations compared to transitions observed in the visible absorption spectra. Above 3 M GuHCl, the curves diverge, and the Fe(II)-CO WT CooA protein shows less change in ellipticity (greater stability) with an increase in GuHCl concentration than the Fe (II) and Fe(III) states. If, as we have supposed, the CD unfolding curve for concentrations greater than 3 M GuHCl primarily reflects signal from the heme domain, the CD data suggest that changes in the coordination state or stability of the heme affect the unfolding and stability of the α-helix in this domain.

The CD data were fitted for the presence of a folding intermediate, and energies were calculated for the process of unfolding from the native state to intermediate, and the intermediate to unfolded state. The three-state fits for the CD curves of Fe(III) WT, Fe(III) F164W, Fe(II), and Fe(II)-CO CooA gave free energy values for the second unfolding step (intermediate → unfolded) that were consistent with those from two-state fits of the visible absorbance unfolding data (Table 1). These results indicate that the second step in the CD unfolding process might be the same as that detected in the visible absorbance unfolding data. The Fe(III) truncated CooA CD unfolding curve was fitted to a two-state model to give a ΔG^{H_2O} of 24 kJ/mol, also consistent with the visible absorbance data for this variant. The stability values for the first step in the CD unfolding process range from 12 to 18 kJ/mol, values that are significantly lower than the energies of the second step. The fits support the conclusion that visible absorbance data report on unfolding of the heme domain, while CD data report on unfolding of both the DNA-binding and heme domains.

Fluorescence Spectra of the Denaturation of Fe(III) WT CooA and Fe(III) F164W CooA Reveal Independent Unfolding of the DNA-Binding Domain. Fe(III) WT CooA fluorescence spectra show an increase in tryptophan fluorescence intensity with increasing concentrations of GuHCl. The native

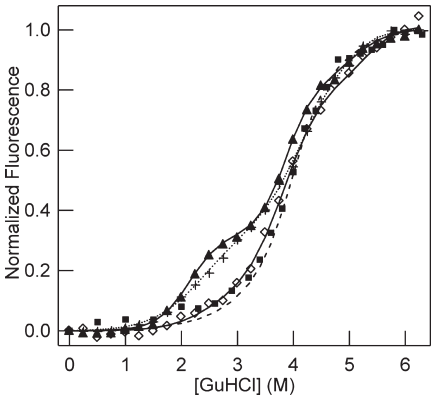

FIGURE 4: Denaturation of WT and F164W CooA monitored by tryptophan fluorescence intensity. Samples of a fixed concentration of CooA (2 μM) were titrated with GuHCl from 0 to 6.25 M and allowed to unfold for 2 h at 25 °C before the fluorescence was measured. The normalized, background-corrected fluorescence intensities at 352 nM at each concentration of GuHCl are plotted. The lines represent fits using a four-state model (see below). Changes in the fluorescence of Fe(III) WT (◇), Fe(III) F164W (▲), Fe(II)-CO F164W (+), and Fe(II)-CO WT (■) CooA as a function of GuHCl are shown.

Fe(III) WT protein has a weak tryptophan fluorescence signal, likely due to heme-induced quenching of fluorescence emission. A quenching effect is not surprising in light of the Fe(II) WT CooA crystal structure, which shows the proximity between the tryptophan residues (Trp^{110}) and the heme cofactors (Figure 1) (*9*). As the protein is exposed to increasing concentrations of GuHCl, the fluorescence intensity increases and the emission maximum shifts from 340 to 352 nm (Figure S2 of the Supporting Information). Similar to observations in the visible absorbance unfolding data of Fe(III) WT CooA, the fluorescence data show a significant change in intensity corresponding to the unfolding transition at GuHCl concentrations of >3 M (Figure 4). As observed in the visible absorbance unfolding curves, fluorescence unfolding curves for titrations of Fe(III) WT CooA at 2 and 4 μM protein were superimposable, while fluorescence unfolding curves collected at 0.5 μM protein showed a shift such that the transition was at lower GuHCl concentrations. The fluorescence unfolding data for Fe(III) WT CooA are similar to data collected by visible absorbance, signifying that fluorescence reports on the folding state of the heme domain.

Since the fluorescence spectra and location of the tryptophan residues of Fe(III) WT CooA suggest that their emission intensity is fully dependent on their proximity to the heme cofactor, fluorescence intensity data for unfolding of the WT protein do not provide any information beyond what is available through visible absorption spectroscopy. To better understand the unfolding behavior of the DNA-binding domain of Fe(III) WT CooA, we unfolded a CooA variant, Fe(III) F164W CooA, that has a substitution to provide an additional tryptophan fluorescence signal in the DNA-binding domain. If the Fe(III) F164W CooA domains unfold independently, the fluorescence denaturation profile would be expected to exhibit two transitions: one for denaturation of the DNA-binding domain due to Trp^{164} and one for unfolding of the heme domain due to Trp^{110}. The fluorescence intensity increases during an unfolding titration of Fe(III) F164W CooA, indicating that in native Fe(III) F164W CooA protein, both Trp^{164} and Trp^{110} are quenched. The fluorescence unfolding profile of Fe(III) F164W CooA shows two significant unfolding transitions (Figure 4). The first unfolding transition of

Fe(III) F164W CooA occurs at concentrations between 2 and 3 M GuHCl. We interpret the first transition to be due to unfolding of the DNA-binding domain of Fe(III) F164W CooA, made apparent by the additional tryptophan signal in the DNA-binding domain. The second transition occurs at GuHCl concentrations of >3 M and is fully coincident with the curve for unfolding of Fe(III) WT CooA. The clear separation of the two transitions suggests that the two domains of Fe(III) F164W CooA are unfolding independently. Furthermore, the coincidence of the unfolding curves above 3 M GuHCl, in both fluorescence and visible absorbance data, further reinforces the interpretation that the heme domain of CooA is unfolding independently at concentrations of >3 M GuHCl.

Changes in Heme Ligation and Activation State Have Little Effect on the Fluorescence Unfolding Curves of WT and F164W CooA. A comparison of the fluorescence unfolding profile of Fe(II)-CO WT CooA with that of Fe(III) WT CooA shows that the curves nearly overlap completely (Figure 4). The difference between the two profiles occurs at high GuHCl concentrations (>4 M GuHCl). Most notably, Fe(III) WT CooA shows a continual fluorescence increase above 5 M GuHCl, while the Fe(II)-CO protein appears to reach a final fluorescence equilibrium and has a post-transition baseline. These results are contrary to the significant differences in unfolding curves that are observed in the visible absorbance unfolding data, but the fluorescence results may be complicated by the fact that in CooA, tryptophan fluorescence emission is a reporter of the environments of both the heme cofactor and the dimer interface (Figure 1D), as discussed in more detail below.

Direct comparison of the fluorescence intensity changes, as represented in Figure 4, may not fully reveal differences in Fe(II)-CO WT and Fe(III) WT CooA unfolding. To interpret the fluorescence unfolding data, it is useful to examine the changes in fluorescence intensity peak maximum wavelength ($\lambda_{max,F}$). Dissociation of CooA into monomers would cause both (i) a significant change in the $\lambda_{max,F}$ as the tryptophans move from a region of low polarity to one that is exposed to solvent (*58*) and (ii) and a moderate increase in tryptophan fluorescence intensity due to an increase in distance from one heme, even if the protein monomers are fully native. Thus, increases in fluorescence intensity that occur upon CooA denaturation may reflect both the unfolding of the protein heme domain and dissociation of the protein from dimers to monomers. A significant increase in fluorescence $\lambda_{max,F}$ for Fe(II)-CO WT CooA occurs between 3 and 4 M GuHCl (Figure S2 of the Supporting Information). Since this change is not coincident with the unfolding transition in the visible absorbance unfolding curve, it is possible that this increase in Fe(II)-CO CooA $\lambda_{max,F}$ is *not* due to unfolding of the heme domain, but to the dissociation of the protein into monomers. The changes in $\lambda_{max,F}$ observed for Fe(III) WT CooA differ considerably from the data for Fe(II)-CO WT CooA, indicating possible differences in GuHCl-dependent dissociation of the dimers into monomers for the two protein activation states. Experiments to examine the dependence of CooA quaternary structure on GuHCl concentration were conducted, but results for these experiments were equivocal (see Materials and Methods).

We investigated the fluorescence unfolding behavior of Fe(II)-CO F164W CooA for comparison to the Fe(III) F164W CooA and Fe(II)-CO WT CooA data. The fluorescence unfolding curve shows two transitions, as observed for unfolding of Fe(III) F164W CooA. Similar to the Fe(III) fluorescence unfolding curve, the first transition for unfolding of Fe(II)-CO F164W CooA is apparent between 2 and 3 M GuHCl. The second transition appears at >3 M GuHCl, and the fluorescence unfolding curves for both states of the WT and F164W proteins are coincident between 3 and 6.25 M GuHCl. These results indicate that the DNA-binding domain of Fe(II)-CO CooA unfolds in a manner independent of the heme domain, and with the same stability that is observed for the Fe(III) state.

The fluorescence data for unfolding of Fe(III) WT, Fe(III) F164W, Fe(II)-CO WT, and Fe(II)-CO F164W CooA were fitted according to a four-state model with two intermediates based on the information gained from all methods of observation. (Fluorescence spectroscopy is not possible for Fe(II) WT CooA due to buffer requirements for a stable Fe(II) state; see Materials and Methods.) In the fits, the presence of two unfolding intermediates was assumed, and fitted energies correspond to transitions from the native folded protein to a first intermediate, from the first intermediate to a second intermediate, and from the second intermediate to the unfolded protein. The four-state fits give stabilities for the first and second transition that are in the range of those from the absorbance and CD-fitted curves (Table 1). Most notably, the fluorescence and CD fits give similar energies for the initial step (range for all fits is 13−18 kJ/mol), which is undoubtedly a measure of the stability of the DNA-binding domain. The second and third steps have a range of stability values for the different heme ligation states, suggesting that either (i) they correspond to different unfolding processes in the various states or (ii) they correspond to processes that are associated with different free energy changes for each protein state.

Use of Variants for Analysis of CooA Unfolding Data. It is possible that the variants unfold in a way that is qualitatively different from that of the WT protein, but this is unlikely for several reasons. First, F164W CooA has CO-dependent activation behavior comparable to that of the WT protein (data not shown), indicating that the variant has the same structure as WT CooA. Also, the Fe(III) F164W CooA visible and CD unfolding data are almost coincident with those for Fe(III) WT for all methods, supporting the conclusions based on the activity data. A crystal structure of the Fe(II) truncate is nearly identical to the structure of the heme domain of the Fe(II) full-length protein (*51*). Furthermore, the similarity of visible unfolding curves for the full-length Fe(III) WT and Fe(III) truncated proteins confirms that the truncate is a good model for the heme domain of the full-length protein.

A Mechanism for CooA Unfolding Includes Multiple Steps. By integrating data from WT, F164W, and truncated CooA, we propose a plausible mechanism for CooA unfolding. A scheme describing this mechanism is shown in Figure 5. Our rationale for including multiple states is given below, followed by a summary of the mechanistic steps. Because CooA is a dimer of monomer units, each with two domains and a noncovalently associated cofactor, the unfolding process is undoubtedly complex. The most salient indicator of multistate unfolding in CooA is the lack of overlap observed in the visible absorbance, fluorescence, and CD unfolding curves for the Fe(III) WT protein (Figure 5). These curves indicate that the unfolding process is not simultaneous for the tryptophan, heme, and α-helix in the protein. Multistate unfolding of CooA is also supported by the apparent presence of nonequilibrium behavior in reversibility experiments (described in Materials and Methods and Figure S3 of the Supporting Information).

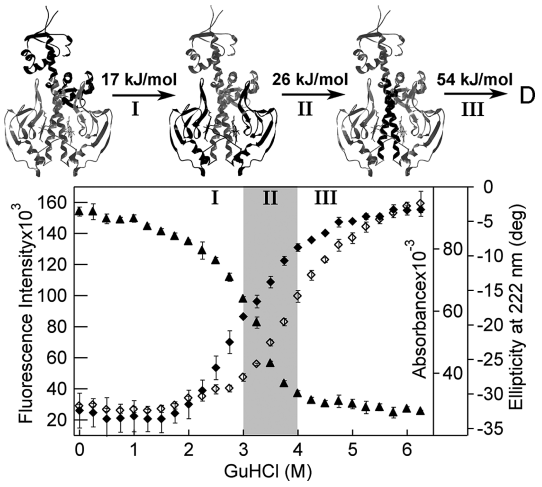

FIGURE 5: Model for denaturation of Fe(III) WT CooA. The averaged raw data as a function of GuHCl concentration collected for Fe(III) WT CooA using fluorescence intensity at 352 nm (◇), absorbance intensity at 424 nm (▲), and CD intensity at 222 nm (◆) are plotted for comparison. The error bars represent the standard deviation for three measurements. Above the chart, the CooA crystal structure is presented with the area unfolded in each step darkened for reference (the protein is presented in the native state for clarity). In step I, between 0 and 3 M GuHCl, the visible absorbance intensity shows a modest decrease. The CD and fluorescence intensities show more significant changes between 2 and 3 M GuHCl. In this step, the protein unfolds from a native state to an intermediate that has an unfolded DNA-binding domain and a mostly native effector domain. The free energy associated with unfolding between steps I and II has been fitted to 17 kJ/mol. In step II, between 3 and 4 M GuHCl, all methods show dramatic changes, indicating that the heme domain unfolds and the protein reaches a second intermediate. The free energy of this step has been fitted to ~26 kJ/mol. In step III, above 4 M GuHCl, the fluorescence continues to increase, which is due to final unfolding of the effector domain and dissociation of the monomers, with a fitted free energy of ~54 kJ/mol. The free energy values are taken from the fits to visible, fluorescence, and CD, as shown in Figures 2–4, and are an approximation of the values derived from all methods and variants of Fe(III) CooA.

In these experiments, the fluorescence refolding behavior of Fe (III) WT CooA is complicated, which may be related to irreversible changes at the heme cofactor. Independent unfolding of individual domains has been reported for several proteins (*41*, *59*–*62*), and the ability of a helix–turn–helix motif to unfold independently has also been studied in some detail (*63*). For CooA, changes in protein secondary structure that occur during the unfolding process between 0 and 3 M are fully reversible and appear to be an independent unfolding event within one domain.

We propose a model in which unfolding of CooA is a four-state process with three distinguishable steps. The first step occurs between 0 and 3 M GuHCl and is due to unfolding of the DNA-binding domain. The visible intensity, CD intensity, and fluorescence intensity of Fe(III) WT CooA show that structural changes affect a region of the protein that is rich in α-helix, but they do not affect the heme (Figure 5). The Fe(III) truncate CooA does not show any change in structure between 0 and 3 M GuHCl (Figures 2B and 3A), confirming that the changes in α-helical content of the protein are not due to unfolding of the heme domain. Both Fe(III) F164W and Fe(II)-CO F164W CooA show an additional unfolding transition between 2 and 3 M GuHCl in the fluorescence profile (Figure 4), likely due to unfolding of the DNA-binding domain made apparent by the tryptophan fluorophore in that domain of the variant. Together, the variant unfolding data confirm that the DNA-binding domain of CooA unfolds at GuHCl concentrations of < 3 M, and the unfolding process of this domain is independent of the activation state of the heme domain.

A second step in CooA denaturation is unfolding of the heme domain. In all states of CooA, the major visible absorbance unfolding transition occurs at GuHCl concentrations of >3 M (Figure 2C), indicating that unfolding of the heme domain occurs within this range of denaturant concentrations. This conclusion is also supported by the observation that the Fe(III) truncate exhibits a minimal change in CD intensity at GuHCl concentrations of < 3 M (Figure 3A). Changes in the ligation state of the heme appear to affect the unfolding stability of the heme domain of CooA. The inactive Fe(III) CooA state shows a visible absorbance unfolding transition between 3 and 4 M GuHCl (Figure 2B), but the Fe(II) and Fe(II)-CO WT CooA states do not show major structural changes until 4 and 5 M GuHCl, respectively (Figure 2C).

A third step likely involves changes in CooA quaternary structure. At GuHCl concentrations of >4 M, after the visible absorbance has reached a post-transition baseline, the Fe(III) WT CooA fluorescence and CD intensities continue to change (Figure 5). These changes are accompanied by an increase in the fluorescence peak maximum at GuHCl concentrations of >4 M (Figure S2 of the Supporting Information), which may be attributable to the dissociation of Fe(III) WT CooA subunits (*58*). Comparison of unfolding profiles at varying protein concentrations (4, 2, and 0.5 μM) confirmed that a dissociation process occurs during denaturation of Fe(III) CooA. At 0.5 μM protein, the major visible and fluorescence transition shifted such that the transition midpoints were at lower GuHCl concentrations (data not shown). These results confirm that a dissociation reaction is influencing the unfolding process of the hemes and tryptophans, which reside at the dimer interface.

If the fluorescence peak maximum is an indicator of quaternary structure in CooA, then we may conclude that Fe(II)-CO WT CooA dissociates into monomers at GuHCl concentrations much lower than those observed for Fe(III) WT CooA. Fe(II)-CO WT CooA shows a change in fluorescence peak maximum wavelength at GuHCl concentrations of < 3 M (Figure S2 of the Supporting Information), a denaturant concentration that is much lower than that necessary to unfold the heme domain as suggested by visible absorbance unfolding curves (Figure 2C). This result has two important implications, which will be discussed below. (i) Although unfolding of CooA is a multistep process for all protein conformations, the order of the individual steps may vary, and (ii) protein–protein interactions at the dimer interface of Fe(II)-CO CooA may be much more sensitive to disruption by denaturant than they are at the interface of Fe(III) CooA.

DISCUSSION

CooA is an exemplary member of two general classes of proteins and has played an important role in the understanding of structure–function relationships in each class. When first crystallized in 2000 (*9*), inactive Fe(II) CooA gave insight into the activation pathway of the CRP/FNR family of transcriptional regulators by representing the only known structure of an inactive state of the family. In addition, the Fe(II) CooA structure was also a major advancement for gas-sensing heme proteins in

that it was the first full-length heme-dependent gas sensor crystallized. For each class, gas sensors and CRP family transcription factors, the main structural features of CooA have been used to posit mechanisms that involve cofactor repositioning, movement at subunit interfaces, rotations of domains, and other detailed structural changes that may accompany activation (*64*). Yet, one issue remains: conclusive structural information exists for only one state of *Rr* CooA, making any proposals regarding allosteric mechanisms speculative. In this work, we approach the question of CooA activation using a different technique that allows for physical comparison of the various activation states of the protein in solution; protein unfolding studies using GuHCl as a chemical denaturant. Our experiments allow us to conclude that activation of CooA occurs with a change in protein stability, but this change is not a reflection of a change in the global stability of the entire protein. Instead, we show through a multistep unfolding mechanism that structural changes may be localized to specific domains and regions of the protein.

Fits to the CooA Unfolding Data Show Consistent Stability of the DNA-Binding Domain and Variable Unfolding of the Heme Domain. On the basis of the four-state model proposed above, we were able to fit the unfolding data for CooA to equilibrium expressions for zero, one, or two intermediates using nonlinear least-squares analysis. We were selective about using a model that best described observed intermediates, multiple unfolding transitions, and reversibility for each protein variant and/or state and method of observation. A comparison of the free energy values obtained is given in Table 1.

The transition that occurs between 2 and 3 M GuHCl ($\Delta G_1^{H_2O}$,CD and $\Delta G_1^{H_2O}$,fluor in Table 1) is attributed to unfolding of the DNA-binding domain of CooA. The free energy of unfolding associated with this transition is consistent and has a value of 16 ± 3 kJ/mol when averaged over all samples and methods. This consistency was wholly unexpected for the three states of CooA. Models for CooA activation suggest that activation of the protein is dependent on a rotation of the DNA-binding domain that repositions recognition helices for proper contact with DNA (*9*). It was assumed that this rotation would require stabilizing contacts with the heme domain such that either the global conformational stability of the protein would change or, at the very least, the DNA domain would be differentially stabilized in one conformation or the other. Instead, the DNA domain appears to act as an independent structural unit with stability that is unchanged by heme coordination changes in the effector domain. Such independent unfolding behavior has been reported for other DNA-binding domains (*59*, *63*). Furthermore, a truncated helix−turn−helix domain has been shown to have very low stability to denaturants (*65*), supporting our finding that the DNA-binding domain of CooA is the least stable structural element.

The effector domain of CooA appears to undergo changes in structural stability upon changes in ligation state, which is reflected in different free energy values for the unfolding process as monitored by visible absorption [Table 1, $\Delta G_2^{H_2O}$,vis for Fe(III) and Fe(II) CooA and $\Delta G_3^{H_2O}$,vis for Fe(II)-CO CooA]. The values derived from fits of the visible absorption data give unfolding energies for the heme domain of the Fe(III), Fe(II), and Fe(II)-CO CooA states in the range of 20−29 kJ/mol. Changes in the stability of heme proteins with changes in heme state, ligation, or heme pocket have been well characterized in cytochrome proteins (*48*, *66*−*69*), and also reported for hemoglobin (*46*, *47*). The differences in the stability of the heme domain among the three states of CooA are smaller than those observed in other heme proteins [$\Delta\Delta G^{H_2O}$ for Fe(III)/Fe(II) cytochrome *c* has been reported to be ∼30 kJ/mol] (*48*, *69*), but unlike single-domain proteins, CooA may be able to compensate for changes in heme ligation by altering contacts at a subunit interface (vide infra). Although there is some inconsistency for CooA in the values calculated for the fluorescence and CD data corresponding to unfolding of the heme domain, these values are consistently significantly greater than any fitted value of $\Delta G_1^{H_2O}$, reinforcing the conclusion that the heme domain unfolding and DNA-binding domain unfolding are distinct processes. Limitations in the analysis may prohibit unequivocal determination of the relative energies of heme domain unfolding in the three states of CooA; however, two conclusions are clear. Changes in heme ligation and activation state affect the structural stability of the heme domain, and the unfolding of this domain occurs in a manner independent of and with a

Table 1: Comparison of Calculated Free Energies for the Various Steps in the Denaturation of CooA

state or protein	probe	$\Delta G_1^{H_2O}$ (kJ/mol) (∼2−3 M GuHCl)	m_1	$\Delta G_2^{H_2O}$(kJ/mol) (∼3−4 M GuHCl)	m_2	$\Delta G_3^{H_2O}$(kJ/mol) (>4 M GuHCl)	m_3
Fe(III) WT	vis[a]			26 (1.1)	8.1 (0.08)		
	CD[a]	18 (0.1)	6.3 (0.8)	28 (1.7)	6.2 (0.4)		
	fluor[a]	16 (3.3)	6.8 (1.6)	24 (3.1)	6.4 (0.8)	54 (7.8)	9.9 (1.1)
Fe(III) F164W	vis[a]			27 (2.5)	7.9 (0.6)		
	CD[b]	12 (0.4)	4.7 (0.1)	29 (2.3)	6.3 (0.8)		
	fluor[a]	13 (5.6)	6.4 (2.4)	28 (8.6)	7.4 (2.2)	51 (9.7)	8.7 (1.3)
Fe(III) truncate	vis[a]			28 (2.7)	7.7 (0.5)		
	CD[c]			24	5.3		
Fe(II)-CO WT	vis[a]					29 (1.3)	7.3 (0.5)
	CD[a]	17 (3.7)	7.0 (1.5)	21 (1.6)	4.7 (0.4)		
	fluor[b]	12 (1.7)	5.6 (1.1)	22 (3.2)	6.8 (1.3)	29 (1.1)	6.2 (0.7)
Fe(II)-CO F164W	fluor[a]	13	6.4	20	5.9	29	6.7
Fe(II) WT	vis[a]			22 (0.1)	5.6 (0.4)		
	CD[b]	16 (0.3)	5.5 (0.2)	46 (0.9)	10.1 (0.9)		

[a] Individual titration curves collected at room temperature were fitted to the appropriate model to yield values for the free energy of unfolding in the absence of denaturant (ΔG^{H_2O}), and the values from three fits were averaged for each unfolding transition with the standard deviation for each transition shown as the error. [b] Free energies are averages of values from two curves with the standard deviation shown as the error. [c] Values represent a single measurement.

change in free energy different from that of the DNA-binding domain.

The nature of the third unfolding process of CooA is more difficult to interpret for the three states of CooA. For Fe(III) WT CooA, we assigned the free energy of the step ($\Delta G_3^{H_2O}$,fluor ~ 54 kJ/mol) to dissociation of the dimer subunits to monomers. In contrast, Fe(II)-CO CooA fluorescence data suggest that in this state of the protein, the subunit dissociation step may occur at lower concentrations of denaturant (Figure S2 of the Supporting Information). For the Fe(II)-CO state, dissociation of subunits would correspond to the process in the fluorescence and CD data that is fitted with $\Delta G_2^{H_2O}$,fluor and $\Delta G_2^{H_2O}$,CD. Accordingly, dissociation of Fe(II)-CO CooA subunits would occur with a change in free energy of 22 kJ/mol, less than half of the value that was calculated for dissociation of subunits of the Fe(III) protein! Interpretation of the Fe(II) CooA unfolding data is even more complicated. Fits for Fe(II) WT CooA give values for $\Delta G_2^{H_2O}$,CD that are much greater than $\Delta G_2^{H_2O}$,vis (46 and 22 kJ/mol, respectively). These results suggest that CD is able to detect a cooperative process in the Fe(II) state that includes both unfolding of the heme domain and dissociation at the subunit interface. Unfortunately, without fluorescence data to describe the dissociation process, it is impossible to relate free energy values to unfolding steps in Fe(II) CooA.

The fluorescence results imply that the mechanism for unfolding of Fe(II)-CO CooA differs from that of the Fe(III) state; in the Fe(II)-CO state, the protein dissociates to monomers before the heme domain undergoes unfolding. The role of the dimer interface in the transmission of the allosteric signal in the CRP/FNR family has been well established (*9*, *23*−*26*, *70*, *71*), and our results support proposals that changes in heme ligation affect subunit interactions and stability at the dimer interface of CooA. Intriguingly, the inactive (effector-free) state of CRP appears to have an unfolding mechanism that is more similar to that of Fe(II)-CO active CooA than it is to that of Fe(III) inactive CooA. It has been shown that inactive CRP unfolds through a mechanism in which dissociation at the dimer interface precedes subunit unfolding (*71*). In this study, the authors fit the inactive CRP unfolding data to obtain free energy values for both the dissociation and unfolding processes. The reported free energy values are comparable to those we obtain for inactive Fe(III) CooA, yet the order of denaturation steps for inactive CRP differs from the order for Fe(III) CooA. This finding may be due to structural differences between inactive Fe(III) CooA, which may be "locked" into an inactive state, and inactive Fe(II) CooA, which may be "poised" for activation and may be more similar to inactive CRP.

Relationship of CooA Structure to Function. Our models for CooA unfolding have interesting implications for the structural differences among the activation states of CooA. We anticipated that that the structural rearrangements that accompany heme coordination changes would be global, and significant differences were anticipated for the stability of the entire protein in each state. Contrary to this expectation, the changes in structural stability that occur with changes in heme coordination are localized to specific regions of the protein. Given that we observe independent stability changes for the domains of CooA, what can be learned about the structural changes that accompany allosteric regulation?

The unfolding data illustrate how activation in CooA is related to changes in protein secondary, tertiary, and quaternary structure. The invariant stability of the DNA-binding domain and the variable stability of the effector-binding heme domain suggest modularity within the protein structure. The DNA-binding domain has a fixed architecture and acts as a unit amidst structural changes in the rest of the protein. In contrast, the heme domain experiences structural changes that affect local stability. From these conclusions, we may speculate about the role of CooA structure in the activation mechanism of the protein. CO binding to the heme of CooA causes significant change in the secondary structure of the heme domain, as is clear from the changes in the stability of this domain. These changes then affect the quaternary structure of the protein by altering contacts at the dimer interface, making the Fe(II)-CO state more susceptible to denaturant-induced dissociation into monomers. The contacts at the dimer interface are then able to influence the protein tertiary structure by repositioning a structurally intact DNA-binding domain. This mechanism is supported by recent CooA crystal structures: they show that the conversion from Fe(II) CooA to Fe(II)-CO CooA occurs with change in the position of the heme cofactor (*11*), and each structure has a different relative orientation of a structurally invariant DNA-binding domain (*9*−*11*).

These observations do not rule out a dynamic mechanism for allostery in CooA. Recently, dynamic models have been proposed to describe activation in allosteric proteins (*72*, *73*). With respect to heme sensor proteins, this theory would predict that when in one heme coordination state, the protein would show a high level of flexibility and would sample multiple conformations on a relatively short time scale. Changes in heme coordination upon gas binding (or release) would cause a "stiffening" of the structure to select for one particular conformational activation state. For CooA, we envision that the inactive Fe(II) state may show dynamic flexibility in the position of the DNA-binding domain, which may sample conformations that are represented in the positions in the Fe(II) CooA crystal structures (*9*, *10*). Binding of CO to CooA may stabilize the active conformation by decreasing the level of motion of the DNA-binding domain and stabilizing a position with exposed F-helices for contact with DNA, as is seen in the crystal structure of a constitutively active CO-bound CooA variant (*11*). Consistent with those proposals, studies have reported on ligand-induced changes in the dynamics of CRP (*74*, *75*). While the studies reported here give no direct evidence for a dynamic mechanism for CooA regulation, dynamic variation of the DNA-binding domain orientation would explain why we were unable to observe three distinct global conformations for CooA: the DNA-binding domain would be equally susceptible to denaturation in each coordination state because its movement would expose the entire domain to solvent.

ACKNOWLEDGMENT

We thank Mary Conrad for constructing the truncated CooA variant, Jose Serate for the purification of F164W CooA, and professors Silvia Cavagnero and Thomas Brunold for the use of their equipment. Finally, we acknowledge Professor M. Thomas Record, Professor Gary Roberts, Dr. Catherine Royer, Professor Karen Fleming, and Jocelyn Pinkert for helpful discussions and critical reading of the manuscript.

SUPPORTING INFORMATION AVAILABLE

Comparison of far UV-CD spectra for Fe(III), Fe(II), and Fe(II)-CO WT CooA and Fe(III) F164W and Fe(III) truncated CooA (Figure S1), changes in the peak maximum of fluorescence

as a function of GuHCl concentration for Fe(III) and Fe(II)-CO WT and Fe(III) F164W and Fe(III) truncate CooA (Figure S2), and reversibility of the unfolding reaction (Figure S3), which compares the fluorescence and CD intensities for forward and reverse titrations of Fe(III) WT CooA with GuHCl. This material is available free of charge via the Internet at http://pubs.acs.org.

REFERENCES

1. Monod, J., Changeux, J. P., and Jacob, F. (1963) Allosteric proteins and cellular control systems. *J. Mol. Biol. 6*, 306–329.
2. Koshland, D. E., Jr., Nemethy, G., and Filmer, D. (1966) Comparison of experimental binding data and theoretical models in proteins containing subunits. *Biochemistry 5*, 365–385.
3. Gilles-Gonzalez, M.-A., and Gonzalez, G. (2005) Heme-based sensors: Defining characteristics, recent developments, and regulatory hypotheses. *J. Inorg. Biochem. 99*, 1–22.
4. Pellicena, P., Karow, D. S., Boon, E. M., Marletta, M. A., and Kuriyan, J. (2004) Crystal structure of an oxygen-binding heme domain related to soluble guanylate cyclases. *Proc. Natl. Acad. Sci. U.S.A. 101*, 12854–12859.
5. Gong, W., Hao, B., and Chan, M. K. (2000) New mechanistic insights from structural studies of the oxygen-sensing domain of *Bradyrhizobium japonicum* FixL. *Biochemistry 39*, 3955–3962.
6. Key, J., and Moffat, K. (2005) Crystal structures of deoxy and CO-bound bjFixLH reveal details of ligand recognition and signaling. *Biochemistry 44*, 4627–4635.
7. Zhang, W., and Phillips, G. N. (2003) Crystallization and X-ray diffraction analysis of the sensor domain of the HemAT aerotactic receptor. *Acta Crystallogr. D59*, 749–751.
8. Zhang, W., Olson, J. S., and Phillips, G. N. (2005) Biophysical and kinetic characterization of HemAT, an aerotaxis receptor from *Bacillus subtilis*. *Biophys. J. 88*, 2801–2814.
9. Lanzilotta, W. N., Schuller, D. J., Thorsteinsson, M. V., Kerby, R. L., Roberts, G. P., and Poulos, T. L. (2000) Structure of the CO sensing transcription activator CooA. *Nat. Struct. Biol. 7*, 876–880.
10. Komori, H., Inagaki, S., Yoshioka, S., Aono, S., and Higuchi, Y. (2007) Crystal structure of CO-sensing transcription activator CooA bound to exogenous ligand imidazole. *J. Mol. Biol. 367*, 864–871.
11. Borjigin, M., Li, H., Lanz, N. D., Kerby, R. L., Roberts, G. P., and Poulos, T. L. (2007) Structure-based hypothesis on the activation of the CO-sensing transcription factor CooA. *Acta Crystallogr. D63*, 282–287.
12. Shelver, D., Kerby, R. L., He, Y., and Roberts, G. P. (1995) Carbon monoxide-induced activation of gene expression in *Rhodospirillum rubrum* requires the product of CooA, a member of the cyclic AMP receptor protein family of transcriptional regulators. *J. Bacteriol. 177*, 2157–2163.
13. Kerby, R. L., Ludden, P. W., and Roberts, G. P. (1995) Carbon monoxide-dependent growth of *Rhodospirillum rubrum*. *J. Bacteriol. 177*, 2241–2244.
14. Korner, H., Sofia, H. J., and Zumft, W. G. (2003) Phylogeny of the bacterial superfamily of Crp-Fnr transcription regulators: Exploiting the metabolic spectrum by controlling alternative gene programs. *FEMS Microbiol. Rev. 27*, 559–592.
15. Aono, S., Ohkubo, K., Matsuo, T., and Nakajima, H. (1998) Redox-controlled ligand exchange of the heme in the CO-sensing transcriptional activator CooA. *J. Biol. Chem. 273*, 25757–25764.
16. Reynolds, M. F., Shelver, D., Kerby, R. L., Parks, R. B., Roberts, G. P., and Burstyn, J. N. (1998) EPR and electronic absorption spectroscopies of the CO-sensing CooA protein reveal a cysteine-ligated low-spin ferric heme. *J. Am. Chem. Soc. 120*, 9080–9081.
17. Clark, R. W., Youn, H., Parks, R. B., Cherney, M. M., Roberts, G. P., and Burstyn, J. N. (2004) Investigation of the role of the N-terminal proline, the distal heme ligand in the CO sensor CooA. *Biochemistry 43*, 14149–14160.
18. Shelver, D., Thorsteinsson, M. V., Kerby, R. L., Chung, S.-Y., Roberts, G. P., Reynolds, M. F., Parks, R. B., and Burstyn, J. N. (1999) Identification of two important heme site residues (cysteine 75 and histidine 77) in CooA, the CO-sensing transcription factor of *Rhodospirillum rubrum*. *Biochemistry 38*, 2669–2678.
19. Dhawan, I. K., Shelver, D., Thorsteinsson, M. V., Roberts, G. P., and Johnson, M. K. (1999) Probing the heme axial ligation in the CO-sensing CooA protein with magnetic circular dichroism spectroscopy. *Biochemistry 38*, 12805–12813.
20. Yamamoto, K., Ishikawa, H., Takahashi, S., Ishimori, K., Morishima, I., Nakajima, H., and Aono, S. (2001) Binding of CO at the Pro2 side is crucial for the activation of CO-sensing transcriptional activator CooA. ^{1}H NMR spectroscopic studies. *J. Biol. Chem. 276*, 11473–11476.
21. Aono, S., Nakajima, H., Saito, K., and Okada, M. (1996) A novel heme protein that acts as a carbon monoxide-dependent transcriptional activator in *Rhodospirillum rubrum*. *Biochem. Biophys. Res. Commun. 228*, 752–756.
22. He, Y., Shelver, D., Kerby, R. L., and Roberts, G. P. (1996) Characterization of a CO-responsive transcriptional activator from *Rhodospirillum rubrum*. *J. Biol. Chem. 271*, 120–123.
23. Moore, L. J., and Kiley, P. J. (2001) Characterization of the dimerization domain in the FNR transcription factor. *J. Biol. Chem. 276*, 45744–45750.
24. Passner, J. M., Schultz, S. C., and Steitz, T. A. (2000) Modeling the cAMP-induced allosteric transition using the crystal structure of CAP-cAMP at 2.1 Å resolution. *J. Mol. Biol. 304*, 847–859.
25. Kerby, R. L., Youn, H., Thorsteinsson, M. V., and Roberts, G. P. (2003) Repositioning about the dimer interface of the transcription regulator CooA: A major signal transduction pathway between the effector and DNA-binding domains. *J. Mol. Biol. 325*, 809–823.
26. Youn, H., Kerby, R. L., Conrad, M., and Roberts, G. P. (2006) Study of highly constitutively active mutants suggests how cAMP activates cAMP receptor protein. *J. Biol. Chem. 281*, 1119–1127.
27. Lazazzera, B. A., Beinert, H., Khoroshilova, N., Kennedy, M. C., and Kiley, P. J. (1996) DNA binding and dimerization of the Fe-S-containing FNR protein from *Escherichia coli* are regulated by oxygen. *J. Biol. Chem. 271*, 2762–2768.
28. Garges, S., and Adhya, S. (1985) Sites of allosteric shift in the structure of the cyclic AMP receptor protein. *Cell 41*, 745–751.
29. Kim, J., Adhya, S., and Garges, S. (1992) Allosteric changes in the cAMP receptor protein of *Escherichia coli*: Hinge reorientation. *Proc. Natl. Acad. Sci. U.S.A. 89*, 9700–9704.
30. Harman, J. G., McKenney, K., and Peterkofsky, A. (1986) Structure-function analysis of three cAMP-independent forms of the cAMP receptor protein. *J. Biol. Chem. 261*, 16332–16339.
31. Ryu, S., Kim, J., Adhya, S., and Garges, S. (1993) Pivotal role of amino acid at position 138 in the allosteric hinge reorientation of cAMP receptor protein. *Proc. Natl. Acad. Sci. U.S.A. 90*, 75–79.
32. Aono, S., Matsuo, T., Shimono, T., Ohkubo, K., Takasaki, H., and Nakajima, H. (1997) Single transduction in the transcriptional activator CooA containing a heme-based CO sensor: Isolation of a dominant positive mutant which is active as the transcriptional activator even in the absence of CO. *Biochem. Biophys. Res. Commun. 240*, 783–786.
33. Won, H.-S., Yamazaki, T., Lee, T.-W., Yoon, M.-K., Park, S.-H., Kyogoku, Y., and Lee, B.-J. (2000) Structural understanding of the allosteric conformational change of cyclic AMP receptor protein by cyclic AMP binding. *Biochemistry 39*, 13953–13962.
34. Baichoo, N., and Heyduk, T. (1999) Mapping cyclic nucleotide-induced conformational changes in cyclic AMP receptor protein by a protein footprinting technique using different chemical proteases. *Protein Sci. 8*, 518–528.
35. Harman, J. G. (2001) Allosteric regulation of the cAMP receptor protein. *Biochim. Biophys. Acta 1547*, 1–17.
36. Schultz, S. C., Shields, G. C., and Steitz, T. A. (1991) Crystal structure of a CAP-DNA complex: The DNA is bent by 90°. *Science 253*, 1001–1007.
37. Passner, J. M., and Steitz, T. A. (1997) The structure of a CAP-DNA complex having two cAMP molecules bound to each monomer. *Proc. Natl. Acad. Sci. U.S.A. 94*, 2843–2847.
38. Aono, S., Takasaki, H., Unno, H., Kamiya, T., and Nakajima, H. (1999) Recognition of target DNA and transcription activation by the CO-sensing transcriptional activator CooA. *Biochem. Biophys. Res. Commun. 261*, 270–275.
39. Pace, C. N., Grimsley, G. R., and Scholtz, J. M. (2005) Denaturation of proteins by urea and guanidine hydrochloride. *Protein Folding Handb. 1*, 45–69.
40. Vijayanathan, V., Greenfield, N. J., Thomas, T. J., Ivanova, M. M., Tyulmenkov, V. V., Klinge, C. M., Gallo, M. A., and Thomas, T. (2007) Effects of estradiol and 4-hydroxytamoxifen on the conformation, thermal stability, and DNA recognition of estrogen receptor β. *Biochem. Cell Biol. 85*, 1–10.
41. Kristl, S., Zhao, S., Falsone, S. F., Somerville, R. L., and Kungl, A. J. (2001) The influence of ATP on the association and unfolding of the tyrosine repressor ligand response domain of *Haemophilus influenzae*. *Biochem. Biophys. Res. Commun. 280*, 81–84.

42. Masino, L., Martin, S. R., and Bayley, P. M. (2000) Ligand binding and thermodynamic stability of a multidomain protein, calmodulin. *Protein Sci. 9*, 1519–1529.
43. Hobson, K. F., Housley, N. A., and Pedigo, S. (2005) Ligand-linked stability of mutants of the C-domain of calmodulin. *Biophys. Chem. 114*, 43–52.
44. Murugan, R., and Mazumdar, S. (2004) Role of substrate on the conformational stability of the heme active site of cytochrome P450cam: Effect of temperature and low concentrations of denaturants. *J. Biol. Inorg. Chem. 9*, 477–488.
45. Lynch, S. M., Boswell, S. A., and Colon, W. (2004) Kinetic stability of Cu/Zn superoxide dismutase is dependent on its metal ligands: Implications for ALS. *Biochemistry 43*, 16525–16531.
46. Puett, D., Friebele, E., and Hammonds, R. G. (1973) A comparison of the conformational stabilities of homologous hemoproteins. Myoglobin from several species, human hemoglobin and subunits. *Biochim. Biophys. Acta 328*, 261–277.
47. Elbaum, D., Pandolfelli, E. R., and Herskovits, T. T. (1974) Denaturation of human and *Glycera dibranchiata* hemoglobins by the urea and amide classes of denaturants. *Biochemistry 13*, 1278–1284.
48. Cohen, D. S., and Pielak, G. J. (1995) Entropic stabilization of cytochrome c upon reduction. *J. Am. Chem. Soc. 117*, 1675–1677.
49. Thorsteinsson, M. V., Kerby, R. L., Youn, H., Conrad, M., Serate, J., Staples, C. R., and Roberts, G. P. (2001) Redox-mediated transcriptional activation in a CooA variant. *J. Biol. Chem. 276*, 26807–26813.
50. Chiang, L. W., Kovari, I., and Howe, M. M. (1993) Mutagenic oligonucleotide-directed PCR amplification (Mod-PCR): An efficient method for generating random base substitution mutations in a DNA sequence element. *PCR Methods Appl. 2*, 210–217.
51. Kuchinskas, M., Li, H., Conrad, M., Roberts, G., and Poulos, T. L. (2006) The role of the DNA-binding domains in CooA activation. *Biochemistry 45*, 7148–7153.
52. Shelver, D., Kerby, R. L., He, Y., and Roberts, G. P. (1997) CooA, a CO-sensing transcription factor from *Rhodospirillum rubrum*, is a CO-binding heme protein. *Proc. Natl. Acad. Sci. U.S.A. 94*, 11216–11220.
53. Smith, P. K., Krohn, R. I., Hermanson, G. T., Mallia, A. K., Gartner, F. H., Provenzano, M. D., Fujimoto, E. K., Goeke, N. M., Olson, B. J., and Klenk, D. C. (1985) Measurement of protein using bicinchoninic acid. *Anal. Biochem. 150*, 76–85.
54. Lundblad, J. R., Laurance, M., and Goodman, R. H. (1996) Fluorescence polarization analysis of protein-DNA and protein-protein interactions. *Mol. Endocrinol. 10*, 607–612.
55. Nozaki, Y. (1972) Preparation of guanidine hydrochloride. *Methods Enzymol. 26*, 43–50.
56. Pace, C. N. (1986) Determination and analysis of urea and guanidine hydrochloride denaturation curves. *Methods Enzymol. 131*, 266–280.
57. Santoro, M. M., and Bolen, D. W. (1988) Unfolding free energy changes determined by the linear extrapolation method. 1. Unfolding of phenylmethanesulfonyl α-chymotrypsin using different denaturants. *Biochemistry 27*, 8063–8068.
58. Lakowicz, J. R. (2006) Principles of Fluorescence Spectroscopy, 3rd ed., Springer, New York.
59. Vreuls, C., Filee, P., Van Melckebeke, H., Aerts, T., De Deyn, P., Llabres, G., Matagne, A., Simorre, J. P., Frere, J. M., and Joris, B. (2004) Guanidinium chloride denaturation of the dimeric *Bacillus licheniformis* BlaI repressor highlights an independent domain unfolding pathway. *Biochem. J. 384*, 179–190.
60. Conejero-Lara, F., Parrado, J., Azuaga, A. I., Smith, R. A., Ponting, C. P., and Dobson, C. M. (1996) Thermal stability of the three domains of streptokinase studied by circular dichroism and nuclear magnetic resonance. *Protein Sci. 5*, 2583–2591.
61. Markovic-Housley, Z., Cooper, A., Lustig, A., Flukiger, K., Stolz, B., and Erni, B. (1994) Independent folding of the domains in the hydrophilic subunit IIABman of the mannose transporter of *Escherichia coli*. *Biochemistry 33*, 10977–10984.
62. Bogusky, M. J., Dobson, C. M., and Smith, R. A. (1989) Reversible independent unfolding of the domains of urokinase monitored by ^{1}H NMR. *Biochemistry 28*, 6728–6735.
63. Religa, T. L., Johnson, C. M., Vu, D. M., Brewer, S. H., Dyer, R. B., and Fersht, A. R. (2007) The helix-turn-helix motif as an ultrafast independently folding domain: The pathway of folding of Engrailed homeodomain. *Proc. Natl. Acad. Sci. U.S.A. 104*, 9272–9277.
64. Roberts, G. P., Kerby, R. L., Youn, H., and Conrad, M. (2005) CooA, a paradigm for gas sensing regulatory proteins. *J. Inorg. Biochem. 99*, 280–292.
65. Felitsky, D. J., and Record, M. T. (2003) Thermal and urea-induced unfolding of the marginally stable lac repressor DNA-binding domain: A model system for analysis of solute effects on protein processes. *Biochemistry 42*, 2202–2217.
66. Bartalesi, I., Bertini, I., Di Rocco, G., Ranieri, A., Rosato, A., Vanarotti, M., Vasos, P. R., and Viezzoli, M. S. (2004) Protein stability and mutations in the axial methionine loop of a minimal cytochrome c. *J. Biol. Inorg. Chem. 9*, 600–608.
67. Sabahi, A., and Wittung-Stafshede, P. (2002) Unfolding the unique c-type heme protein *Chlamydomonas reinhardtii* cytochrome f. *Biochim. Biophys. Acta 1596*, 163–171.
68. Wittung-Stafshede, P., Lee, J. C., Winkler, J. R., and Gray, H. B. (1999) Cytochrome b562 folding triggered by electron transfer: Approaching the speed limit for formation of a four-helix-bundle protein. *Proc. Natl. Acad. Sci. U.S.A. 96*, 6587–6590.
69. Pascher, T., Chesick, J. P., Winkler, J. R., and Gray, H. B. (1996) Protein folding triggered by electron transfer. *Science 271*, 1558–1560.
70. Polit, A., Bonarek, P., Kepys, B., Kedracka-Krok, S., Gorecki, A., and Wasylewski, Z. (2003) Kinetic studies of cAMP-induced allosteric changes in mutants T127I, S128A, and T127I/S128A of the cAMP receptor protein from *Escherichia coli*. *J. Biol. Chem. 278*, 43020–43026.
71. Cheng, X., Gonzalez, M. L., and Lee, J. C. (1993) Energetics of intersubunit and intrasubunit interactions of *Escherichia coli* adenosine cyclic 3′,5′-phosphate receptor protein. *Biochemistry 32*, 8130–8139.
72. Kern, D., and Zuiderweg, E. R. P. (2003) The role of dynamics in allosteric regulation. *Curr. Opin. Struct. Biol. 13*, 748–757.
73. Cooper, A., and Dryden, D. T. F. (1984) Allostery without conformational change. A plausible model. *Eur. Biophys. J. 11*, 103–109.
74. Dong, A., Malecki, J. M., Lee, L., Carpenter, J. F., and Lee, J. C. (2002) Ligand-induced conformational and structural dynamics changes in *Escherichia coli* cyclic AMP receptor protein. *Biochemistry 41*, 6660–6667.
75. Popovych, N., Sun, S., Ebright, R. H., and Kalodimos, C. G. (2006) Dynamically driven protein allostery. *Nat. Struct. Mol. Biol. 13*, 831–838.